# AI-Driven Change Detection: Enhancing Urban Planning with Advanced Change Detection Models in High-Resolution Satellite Imagery

**Sai Rishyanth Visinigiri[1*], Kavya Reddy Vutukuri[1], A L Amutha[1], L Krishnaraj[2]**

[1]Department of Computational Intelligence, SRM Institute of Science and Technology, Kattankulathur, Chengalpattu, Tamil Nadu 603203, India

[2]Department of Civil Engineering, SRM institute of Science and Technology, Kattankulathur, Chennai, Tamil Nadu, 603203, India

*Corresponding author Email: visinigiririshyanth@gmail.com

---------------------------------------------------------------***---------------------------------------------------------------

**Abstract -** This research compares traditional change detection (CD) methods, including PCA and k-Means, with advanced approaches using fully convolutional neural networks (FCNNs) for detecting changes in urban and suburban satellite imagery. Aligned with SDG 11 (Sustainable Cities and Communities), it emphasizes the importance of robust CD algorithms for sustainable urbanization and resilient infrastructure. Inefficient detection methods complicate tracking urban expansion, deforestation, and environmental degradation, potentially delaying responses to disasters and undermining resource management. The study evaluates unsupervised models using PCA and k-Means alongside FresUNet-based architectures and Siamese networks tailored for urban planning. Traditional methods often neglect spatial-temporal dynamics critical for accurate detection. In contrast, the Siamese UNet model, incorporating attention mechanisms, excels in identifying subtle changes while minimizing noise, significantly enhancing detection accuracy and aiding disaster risk reduction. Performance evaluation spans diverse data sources, including UAVs, IoT devices, and large-scale Earth observation systems like Copernicus and Landsat. The goal is to identify the most effective algorithm for varied datasets. The Onera Satellite Change Detection (OSCD) dataset, featuring 24 pairs of multispectral Sentinel-2 images from 2015–2018 across Brazil, the U.S., Europe, the Middle East, and Asia, is used for training. This dataset includes 13-band images with pixel-level ground truth for urban changes, offering resolutions of 10 m, 20 m, and 60 m. By leveraging high-resolution data and advanced architectures, this research aims to address critical challenges in environmental monitoring and urban planning.

## 1. INTRODUCTION

Urbanization, driven by high land pressure, low agricultural incomes, and rapid population growth in many developing countries, is both a catalyst for human development and a source of substantial challenges. Uncontrolled urbanization results in substandard living conditions, pollution, waste management crises, and traffic congestion (Karakayaci & Zuhal.2016; Bhatta, Basudeb. 2012; Coisnon, Thomas & Oueslati, Walid & Salanié, Julien. 2013). Technological solutions are urgently needed to address these issues and ensure equitable development. Rapid transformations in urban environments, fueled by population growth and infrastructure expansion, pose significant challenges in monitoring and managing effectively. Without reliable tools to detect and analyze these changes, urban planning risks becoming reactive, leading to unsustainable outcomes. Robust change detection models offer critical insights, enabling proactive and sustainable urban development.

The problem of change detection is one of classification. As image processing and computer vision advanced, so did this classic problem in earth observation image analysis. Cloud detection, road and building appearance, disaster response and recovery, time series analysis, monitoring of agricultural crops or deforestation, etc. are some of the different changes that are examined. In practice, a change map (CM) is computed by taking two co-registered images, say $I_1$ and $I_2$, that have the same area and size (M x M pixels). A positive label on the change map (CM), which is a binary map, indicates the region where a pixel's value is 1 (white) when a change between $I_1$ and $I_2$ is detected, and 0 (black) otherwise.

Traditional change detection methods in remote sensing primarily focused on preprocessing multi-temporal images to address distortions such as geometric misalignments and atmospheric interference (Cheng G et al.,2024). Statistical validation was emphasized to ensure accuracy (Aldoski et al., 2013). Techniques such as unsupervised clustering(M. Hao et al., 2014), which grouped pixels based on spectral properties, enhanced detection but were susceptible to noise and required careful parameter tuning (Bruzzone & Prieto, 2000 ; He, P. et al.,2021 ). Object-based methods improved performance in heterogeneous environments by incorporating spatial context, although they were computationally intensive and dependent on image quality (Hussain et al., 2013). Advanced systems combined multiple classifiers to leverage spectral and spatial features, emphasizing the significance of parameter optimization for balancing accuracy and efficiency (Tan et al., 2024). However, traditional methods encountered limitations such as sensitivity to noise, high computational demands, and challenges with low-quality images.

Various approaches have been explored to enhance accuracy in machine learning for change detection (R. L. Lillestrand et al.,1972). Supervised classification using decision trees monitors seasonal variations and ecological changes but faces challenges in urban or agricultural settings due to data availability concerns (Goswami, A. et al., 2022; J. L. H. Alvarez et al.,2020).Advanced techniques, such as integrating spectral indices with Markov Random Fields, incorporate spatial dependencies and effectively address noise from varying spectral properties. Mahalanobis distance combined with PCA has been utilized for change detection, but struggles to distinguish subtle changes due to spatial resolution limitations (Im & Jensen, 2005; Lu et al., 2008; Zelinski et al., 2014). More sophisticated methods, like Conditional Random Fields (CRFs), enhance spatial accuracy but require high-quality labeled data and computational resources Fusion techniques combine data sources, like Synthetic Aperture Radar (SAR) and multispectral images, to augment detection precision but demand intricate preprocessing ( J. Zhang et al.,2022). Integration of spectral indices with models like Markov Random Fields addresses noise by incorporating spatial dependencies, improving detection in noisy environments. Integration of remote sensing data with Geographic Information System (GIS) tools provides valuable insights for land cover changes but is often limited by temporal coverage and varying image quality (Seo et al., 2009; Chen, 2002; Zhou et al., 2016). Interactive learning approaches that integrate user feedback refine detection models but are limited by expert knowledge (Saux & Randrianarivo, 2013).

Neural networks have significantly advanced remote sensing-based change detection by enhancing accuracy and robustness. Deep learning models, such as U-Net, enhanced with early fusion techniques and Siamese U-Net architectures incorporating attention mechanisms, excel in complex detection scenarios. Recurrent Neural Networks (RNNs) with LSTM units effectively model temporal changes, although they require extensive labeled data and robust preprocessing (Ouerghi, 2022; Chen et al., 2022; Lyu & Lu, 2016). Combining neural networks with Geographic Information System (GIS) data has demonstrated success in forecasting land use changes, while multiclass and binary classification models enhance high-resolution segmentation, albeit increasing model complexity and the risk of overfitting (Pijanowski et al., 2002; Zheng & Chen, 2021; Cai et al., 2020). DenseNets have proven effective in landslide detection by integrating environmental factors, but they rely on high-quality data. Conditional Variational Autoencoders (CVA) with adversarial training offer robust classification of hyperspectral imagery, albeit at high computational costs. Convolutional Neural Networks (CNNs) have demonstrated utility for urban change detection, but challenges in generalization persist, which can be addressed through transfer learning. Although effective for similarity detection, encounter difficulties with data generalization, emphasizing the necessity for improved data augmentation strategies (Daudt et al., 2018; Wang et al., 2020; Zagoruyko & Komodakis, 2015).

This research aims to revolutionize urban planning by leveraging advanced change detection models. Through a thorough comparative analysis of fully convolutional

neural network (FCNN) architectures and conventional change detection methods, we seek to identify the most effective algorithm for monitoring urban development. Our primary focus is on detecting changes in urban areas, which will enable precise identification and tracking of urban sprawl and shifts in land use. These insights will provide invaluable guidance for sustainable urban growth. The outcomes of this study will significantly contribute to optimizing urban planning processes, enhancing infrastructure management, and promoting environmentally responsible development.

## 2. CHANGE DETECTION METHODS

The process begins with two co-registered images, captured at different time intervals, being provided as input to the change detection model. The model analyzes changes between the input images, identifying significant variations. The results are then refined into a detailed change map, visually highlighting areas of transformation and providing actionable insights for urban planning and decision-making.
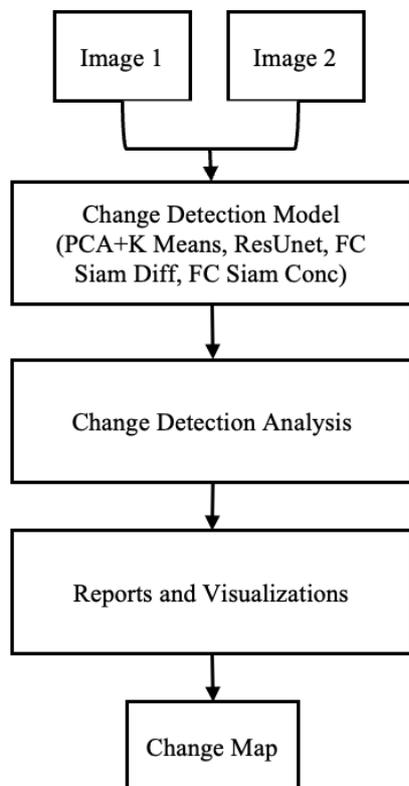


Fig-1: Change Detection Process Flow

### A. Unsupervised model using PCA and K-Means Clustering

An effective approach to detecting changes between two images is to use unsupervised machine learning techniques, such as Principal Component Analysis (PCA) and K-Means clustering (Celik, 2009). These techniques combine dimensionality reduction and clustering to identify significant changes in image data.

Consider two co registered satellite images, $I_1$ and $I_2$, captured at two different times, $t_1$ and $t_2$, of size H x W. The first step is to generate a difference image $I_d$ by calculating the absolute pixel-wise difference between $I_1$ and $I_2$:

$$\mathbf{I_d = |\, I_2 - I_1 \,|}$$

The difference image $I_d$ is divided into h x h non overlapping blocks where $h \geq 2$ to extract localized information. Let $I_d(y, x) = \{i_d(m, n) | y - \lceil h/2 \rceil + 1 \leq m \leq y + h - \lceil h/2 \rceil, x - \lceil h/2 \rceil + 1 \leq n \leq x + h - \lceil h/2 \rceil\}$ be $h \times h$ difference-image block referenced by (centered at when h is odd) coordinates (y, x), where $\lceil \; \rceil$ is a mathematical ceiling operator which rounds a number up, to the nearest integer, e.g., $\lceil 4.5 \rceil = 5$. For each block centered at pixel (y, x), the block vector $i_d(y, x)$ is formed by lexicographically ordering the pixel values in that block. To reduce dimensionality, PCA is applied to the vectors from each block. The covariance matrix C is computed, and its eigenvectors $e_s$ and eigenvalues $\lambda_s$ are derived:

$$\mathbf{C = \frac{1}{M} \sum_{p=1}^{M} \Delta_p \Delta_p^T}$$

Where $\Delta_p = i_d^p - \Psi$, and $i_d^p$ is used to denote the vector $i_d(y, x)$, while p represents an index with $1 \leq p \leq M = \lfloor (H \times W)/(h \times h) \rfloor$, where $\lfloor \; \rfloor$ is a mathematical floor operator which rounds a number down, to the nearest integer. The average vector of the set is defined by

$$\mathbf{\Psi = \frac{1}{M} \sum_{p=1}^{M} i_d^p}$$

The eigenvectors corresponding to the largest eigenvalues are selected to create an eigenvector space. Each pixel's feature vector is projected onto this space to obtain a reduced feature vector

$$\mathbf{v\,(i, j) = [v_1, v_2 \ldots, v_S]^T \text{ with } v_s = e_s^T(i_d(i, j) - \Psi)}$$

The feature vectors are clustered into two classes—changed ($w_c$) and unchanged ($w_u$)—using the k-means clustering algorithm with k=2. The mean feature vectors for each cluster, $v_{w_c}$ and $v_{w_u}$ are calculated. To label the clusters, the cluster with the lower average intensity in the difference image is assigned as $w_u$ (unchanged), while the other is assigned as $w_c$ (changed).

Using the mean feature vectors of the two clusters $v_{w_c}$ (changed class) and $v_{w_u}$ (unchanged class), a binary change map CM is created for the entire image. Each pixel is classified based on which cluster its feature vector v (i, j) is closer to in terms of Euclidean distance

$$cm(i, j)= \begin{cases} 1, & \| v(i,j) - v_{w_c} \|_2 \le \| v(i,j) - v_{w_u} \|_2 \\ 0, & \text{otherwise} \end{cases}$$

where $\|.\|_2$ represents the Euclidean distance and cm(i, j) = 1 is the pixel in the change region and cm(i, j) = 0 is the pixel in the unchanged region.
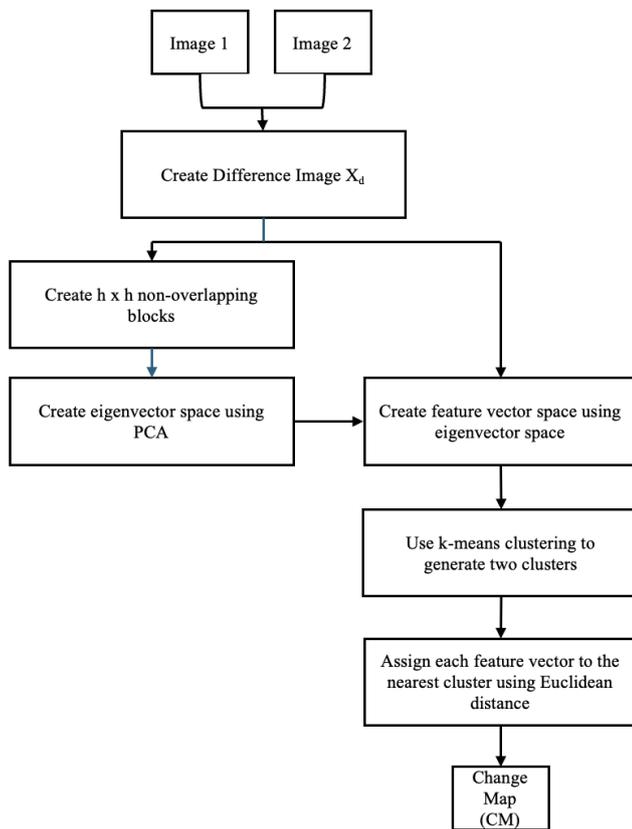


Fig-2: Unsupervised Model using PCA and k-Means

### B. FresUNet Model

FresUNet, a novel architecture, excels at change detection in multi-temporal satellite imagery. It concatenates multi-temporal patches during training and testing along the channel dimension, enabling the network to analyze combined information from two different time points. Consider a pair of patches, $(P_{t1}^{i,j}, P_{t2}^{i,j})$, extracted from images, $I_{t1}^i$ and $I_{t2}^i$. Each patch has dimensions h×w×c. The input to FresUNet has dimensions h×w×2c,

processing both patches simultaneously and enhancing change detection.

### 1. Encoder Architecture

Once the input is prepared, it is fed into the encoder section of the network, which consists of several residual blocks followed by subsampling residual blocks. Each residual block includes a combination of convolutional layers, specifically Conv3×3, followed by batch normalization (BN) and ReLU activation functions. The structure of a single residual block can be expressed as:

$$R(x)=BN(ReLU(Conv3\times3(x)))+x$$

where R(x) denotes the output of the residual block, and x is the input feature map. This architecture helps in mitigating the vanishing gradient problem, allowing for deeper networks to be trained effectively.
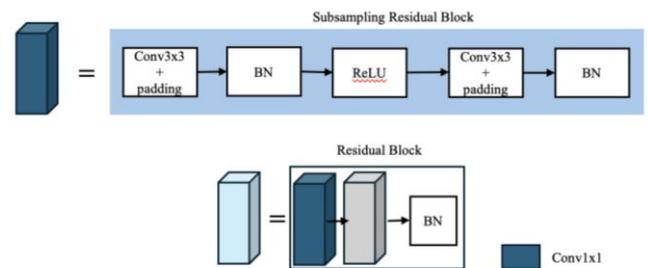


Fig-3: Subsampling Residual Block of FresUNet

### 1. Decoder Architecture

After processing through the encoder, the feature maps are passed to the decoder part of the FresUNet. This section similarly consists of residual blocks, but it incorporates up sampling residual blocks that use transpose convolution layers TrConv3×3 instead of standard convolution layers. The structure for an up sampling residual block can be formulated as:

$$U(x)=BN(ReLU(TrConv3\times3(x)))+x$$

Here, U(x) represents the output of the up sampling residual block, effectively reconstructing the spatial dimensions of the feature maps as they are processed back to the output layer.
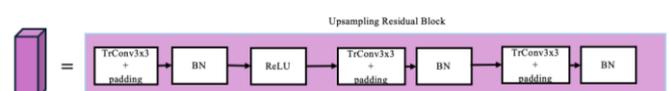


Fig-4: Upsampling Residual Block of FresUNet

At the end of the decoding phase, the output from the decoder, denoted as $x_i$, undergoes a log softmax activation function to produce the predicted change map $CM_i$. The mathematical representation of the log softmax function is given by:

$$LogSoftmax(x_i)=\log\left(\frac{e^{x_i}}{\sum_j e^{x_j}}\right)$$

This output provides a probabilistic representation of the detected changes, enabling the model to classify each pixel effectively. To update the weights of the network during the training phase, FresUNet employs the negative log likelihood loss function, which can be mathematically expressed as:

$$L= - \sum_i y_i \log (CM_i)$$

where $y_i$ represents the ground truth labels, and $CM_i$ is the predicted change map. This loss function drives the optimization process, guiding the network to minimize discrepancies between the predicted and actual outputs.
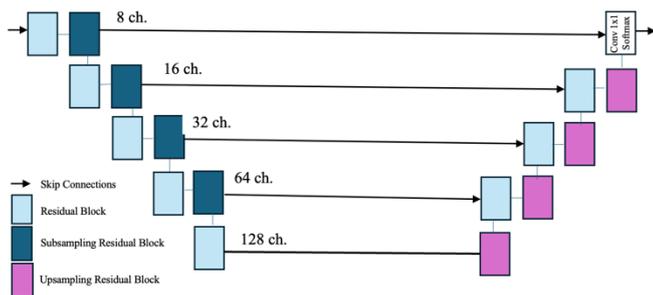


Fig-5: FresUNet Model Architecture

**C. Fully Convolutional – Siamese (FC-Siam):**

This system extends UNet based architecture using a Siamese network with two branches for feature extraction, sharing weights between branches. It includes two variants:

- **FC-Siam-Concatenated**: Concatenates skip connections from each branch during decoding.

- **FC-Siam-Difference**: Uses absolute differences between skip connections.

Both FC-Siam architectures perform similarly in real-time applications.

FC-Siam is a natural extension of the FresUNet architecture, leveraging a Siamese-based structure for improved change detection in multi-temporal satellite imagery. Unlike FresUNet, which concatenates patches

from two different time points along the channel dimension, FC-Siam processes the patches through two parallel encoder branches with shared weights. This Siamese architecture enables the network to independently extract features from each input time point before combining them for change detection, enhancing the model's ability to capture subtle temporal variations.

In FC-Siam, the two branches receive patches ( $P_{t1}^{i,j}, P_{t2}^{i,j}$ ), extracted from extracted from images, $I_{t1}^i$ and $I_{t2}^i$, respectively. Each branch processes its input through identical encoder networks with shared parameters, ensuring consistent feature extraction across both time points. The outputs of the encoder branches are then combined in the feature fusion stage and passed to the decoder for final reconstruction and change detection. This structure promotes a more effective representation of temporal differences by focusing on features unique to each time point while suppressing irrelevant information.

Two primary variants of FC-Siam are explored for feature fusion: FC-Siam-Concatenation and FC-Siam-Difference. In FC-Siam-Concatenation, the feature maps from both encoder branches are concatenated before being passed into the decoder. This approach allows the model to learn a joint representation of both time points, capturing complementary information to detect changes. On the other hand, FC-Siam-Difference computes the absolute difference between the feature maps from the two branches. These variant highlights areas of change more explicitly, reducing redundant information and enhancing sensitivity to differences between the two time points.

The decoder architecture in FC-Siam follows the same design principles as FresUNet, utilizing up sampling residual blocks with transpose convolutions to reconstruct the spatial dimensions and generate the final change map. The output of the decoder undergoes a log SoftMax activation function to produce a probabilistic change map. For training, the network employs the negative log likelihood loss function, ensuring that the predicted change map closely aligns with the ground truth labels.
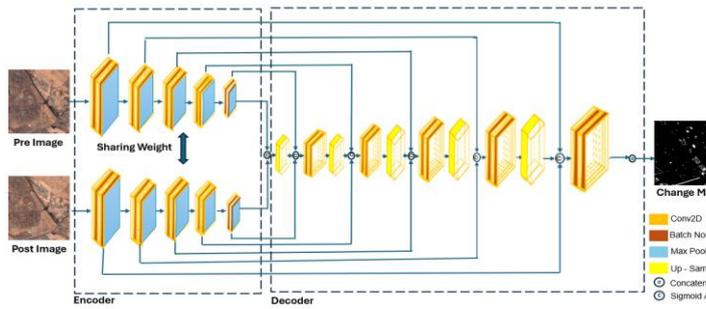
Fig-6: Siamese based UNet Architecture

## 3. EXPERIMENTS

In this section, the dataset used for evaluation, the custom model configuration and the performance metrics for the different change detection models is described.

### A. Dataset

The evaluation of the various change detection models is done on the widely used benchmark ONERA dataset. ONERA dataset consists of 24 pairs of multispectral images along with their ground truth pixel annotations taken from the Sentinel-2 satellites between 2015 and 2018. By following the ONERA creator's guidelines, split the dataset into train and test set. The training set consists of 14 pair of images and the testing set consists of 10 pair of images. These images vary in size and spatial resolution between 10m, 20m and 60m.

Table-1: Sentinnel-2 Satellite 13 bands

| Sentinel -2 Bands | Central Wavelength (nm) | Resolution (m) |
|---|---|---|
| Band 1 – Coastal Aerosol | 443 | 60 |
| Band 2 – Blue | 490 | 10 |
| Band 3 – Green | 560 | 10 |
| Band 4 – Red | 665 | 10 |
| Band 5 – Vegetation Red Edge | 705 | 20 |
| Band 6 - Vegetation Red Edge | 740 | 20 |
| Band 7 - Vegetation Red Edge | 783 | 20 |
| Band 8 – NIR | 842 | 10 |
| Band 8A - Vegetation Red Edge | 865 | 20 |
| Band 9 – Water Vapor | 940 | 60 |
| Band 10 – SWIR - Cirrus | 1375 | 60 |
| Band 11 - SWIR | 1610 | 20 |
| Band 12 - SWIR | 2190 | 20 |

### B. Settings

In this study, a custom configuration was employed for analysing multispectral Sentinel-2 imagery. The model was set to operate without prototype testing (IS_PROTOTYPE = False), with a tuning parameter of FP_MODIFIER = 10 to optimize performance. The batch size was set to 32, and each input patch had dimensions of 96×96 pixels. The training spanned 50 epochs, incorporating data normalization (NORMALISE_IMGS = True) to enhance input consistency. A training stride of 47 pixels, calculated as PATCH_SIDE/2 - 1, was used.

The input type focused on all 13 spectral bands from Sentinel-2 imagery (Type 3). The model performed better with all 13 bands, reducing fluctuations in change detection compared to other architectures. Dataset augmentation was applied to enrich training data (AUG = True), with no pre-trained models loaded for this experiment (TRAINED = False).

All methodologies were implemented in Python 3.8.10 with PyTorch on a workstation featuring an Intel Core i5-1335U processor and Intel Iris Xe Graphics. Comparative analysis was conducted with PCA, K-Means, FC-Siam-Conc, FC-Siam-Diff, and FresUNet architectures.

### C. Performance Metrics

In change detection with limited labeled data, precision, recall, and F1 score are crucial. Precision measures true positive predictions among positives, indicating reliability and avoiding false positives. Recall assesses true positives among actual positives, highlighting effectiveness in identifying real changes. F1 score, the harmonic mean of precision and recall, balances false positives and negatives, especially in imbalanced datasets.

$$\text{Precision} = \frac{TP}{TP + FP}$$

$$\text{Recall} = \frac{TP}{TP + FN}$$

$$F1 = 2 \times \frac{\text{Precision x Recall}}{\text{Precision + Recall}}$$

$$Accuracy = \frac{TP + TN}{TP + TN + FP + FN}$$

Where, TP is True Positive, TN is True Negative, FP is False Positive and FN is False Negative.

## 4. RESULTS

This section presents the evaluation metrics for four different models to change detection on the OSCD dataset. Table 2 summarizes these metrics for the evaluated models.

Table-2: Evaluation Metrics on Change Detection Dataset

| Data | Network | Precision | Recall | Accuracy | F1 Score |
|---|---|---|---|---|---|
| OSCD 13 bands | PCA, K-Means | 33.23 | 33.01 | 85.04 | 33.08 |
| | FresUNet | 16.9 | **77.85** | 79.33 | 27.77 |
| | FC-Siam-conc | 34.04 | 26.88 | 93.59 | 30.03 |
| | FC-Siam-diff | **45.31** | 30.81 | **94.56** | **36.67** |

Given the limited labeled data in the OSCD dataset, accuracy isn't suitable for this experiment. Instead, precision, recall, and F1 score are used to evaluate the model's effectiveness in change detection, addressing both detection and misclassification.

### A. Performance Analysis for PCA and k-Means Model



Abu Dhabi 2016　　　Abu Dhabi 2018　　　Change Map

Fig-8: Change Detection using PCA and k-Means Clustering

The PCA and k-means model for urban change detection face challenges, with a precision of 33.23 and a recall of 33.01. This indicates a high frequency of false positives and missed changes. While the accuracy is 85.04, the F1 score of 33.08 underscores the poor balance between precision and recall, suggesting ineffective change identification.

Low precision and recall are attributed to urban noise, the lack of spatial context in PCA, and k-means' inability to distinguish growth from artifacts. Enhancing data quality and adopting improved methodologies are essential for enhanced performance.



Abu Dhabi 2016.　　Abu Dhabi 2018　　　New Change Map

Fig-9: Change Detection for modified image using PCA and k-Means Clustering

Black pixel occlusion significantly hinders change detection by creating data voids. This causes the model to misinterpret the absence of data as no change, masking underlying features and preventing the model from detecting true modifications. Consequently, clear, unobstructed data is crucial for reliable results.

### B. Performance Analysis for FresUNet Model

The FresUNet model for change detection has a mixed performance profile. It has a precision of 16.9%, recall of 77.85%, accuracy of 79%, and an F1 score of 27.77. This means that only about 16.9% of the changes identified by the model are accurate, leading to many false positives.



Image 1　　　　　Image2.　　　　Change Map

Fig-10: Change Detection using FresUNet Model

Here, Black is True Negative, White is True Positive, Green is False Positive and Magenta is False Negative.

A recall of 77.85 shows the model accurately captures changes, but its low precision causes many false positives. 79% accuracy indicates most areas remain unchanged, while the F1 score of 27.77 shows poor precision-recall trade-off. Improving FresUNet's reliability requires better noise differentiation.

## C. Performance Analysis for Fully Convolutional Siamese based UNet Model

### i. Fully Convolutional Siamese Concatenated Model (FC Siam-Conc)

The FC Siam-Conc model shows balanced performance with 34.04 precision, 26.88 recall, 93.59 accuracy, and an F1 score of 30.03. While one-third of detected changes are accurate, only a quarter of actual changes are captured, missing many genuine ones. The high accuracy likely reflects predominantly unchanged areas.



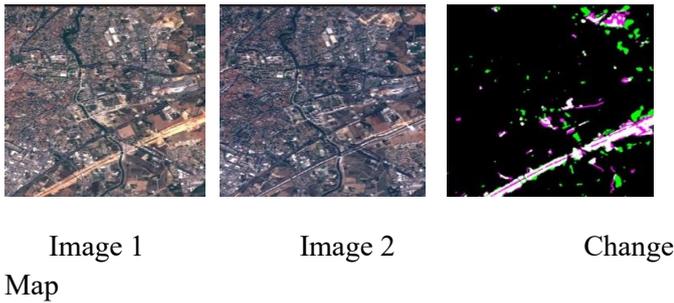Image 1          Image 2          Change Map

Fig-11: Change Detection using FC Siam-Conc

Here, Black is True Negative, White is True Positive, Green is False Positive and Magenta is False Negative.

The FC Siam model outperforms PCA-K-means with higher precision, reducing false positives and offering better boundary delineation. Compared to FresUNet, it balances precision and recall more effectively, though recall remains lower. FresUNet captures more changes but produces more false positives. With 93.59% accuracy, FC Siam is more reliable for tasks prioritizing precision, though recall improvements are needed for optimal urban change detection.

### ii. Fully Convolutional Siamese Difference Model (FC Siam-Diff)

The FC Siam Diff model for change detection performs well, with a precision of 45.31, recall of 30.81, accuracy of 94.56, and an F1 score of 36.67. This higher precision indicates the model minimizes false positives, making it more reliable for accurate change detection.
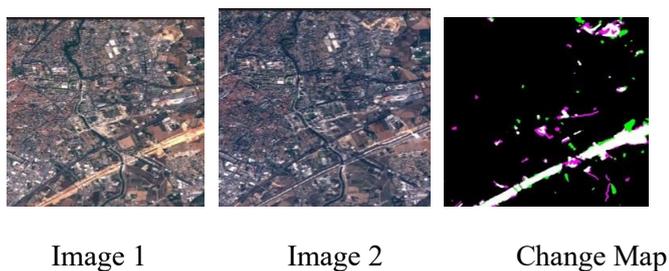


Image 1          Image 2          Change Map

Fig-11: Change Detection using FC Siam-Diff

Here, Black is True Negative, White is True Positive, Green is False Positive and Magenta is False Negative.

The recall of 30.81 shows FC Siam Diff captures more true changes than FC Siam Conc, though it still misses many. Its 94.56% accuracy may be inflated by unchanged areas, but the F1 score of 36.67—the highest among the models—reflects a better balance between precision and recall. This makes FC Siam Diff more effective at reducing false positives and improving overall change detection.

## 5. CONCLUSIONS

This study compared four models for urban change detection: PCA with k-means, FresUNet, FC-Siam-Conc, and FC-Siam-Diff. The PCA and k-means model exhibited low precision (33.23) and recall (33.01), resulting in an F1 score of 33.08, indicating high sensitivity to noise and frequent misclassifications. FresUNet achieved a high recall of 77.85 but suffered from a low precision of 16.9, with an F1 score of 27.77 due to a significant number of false positives. The FC-Siam-Conc model provided a more balanced performance with a precision of 34.04, recall of 26.88, and an F1 score of 30.03, although it missed many genuine changes. In contrast, the FC-Siam-Diff model outperformed others with a precision of 45.31, recall of 30.81, and the highest F1 score of 36.67, minimizing false positives while maintaining a high accuracy of 94.56. Among the models, FC-Siam-Diff emerged as the most reliable for urban change detection. Future research should focus on improving recall and exploring larger, more diverse datasets to enhance the overall performance further.

## 6. FUTURE WORKS

The proposed system possesses substantial potential, but it requires further enhancements to optimize its effectiveness. Future endeavors will concentrate on developing an interactive web platform for real-time change detection. This platform will facilitate the seamless upload of diverse data sources, including satellite imagery and drone footage, thereby providing a user-friendly interface for applications such as urban development monitoring and infrastructure management.

Expanding data source integration is paramount for comprehensive analysis. Integrating aerial imagery, ground-based sensor data, and Internet of Things (IoT)

devices will significantly broaden the system's capabilities. For instance, the fusion of real-time traffic camera imagery with historical satellite data can empower city planners to analyze urban infrastructure and traffic patterns with greater precision.

The platform can also benefit from the incorporation of sophisticated analytical tools that provide detailed insights. These tools can support a wide range of use cases, including assisting healthcare providers in detecting substantial alterations in medical images and enabling farmers to monitor seasonal crop variations. Customizable visualizations and statistical tools will facilitate data interpretation and decision-making.

User-centric design and continuous feedback mechanisms are indispensable to ensure that the platform aligns with user requirements. Collaborating with target users, such as farmers or environmental scientists, during the design process will facilitate the refinement of features tailored to specific applications. Regular feedback collection will enhance usability and promote widespread adoption across diverse sectors.

Finally, exploring multi-band image analysis will substantially enhance change detection accuracy. Utilizing visible, infrared, and thermal bands will enable more comprehensive assessments. Environmental scientists can monitor vegetation health using near-infrared data, while urban planners can identify heat islands through thermal imagery. This multi-band approach will significantly expand the system's applicability across various industries.

# 7. REFERENCES

1. Aldoski, Jwan & Mansor, Shattri & Shafri, Helmi & Shafri, Mohd. (2013). Change Detection Process and Techniques.
2. Bruzzone and D. Prieto, "Automatic analysis of the difference image for unsupervised change detection," *IEEE Trans. Geosci. Remote Sens.*, vol. 38, no. 3, pp. 1171–1182, May 2000.
3. M. Hussain, D. Chen, A. Cheng, H. Wei, and D. Stanley, "Change detection from remotely sensed images: From pixel-based to object-based approaches"
4. K. Tan, X. Jin, A. Plaza, X. Wang, L. Xiao, and P. Du, "Automatic change detection in high-resolution remote sensing images by using a multiple classifier system and spectral-spatial featureS"
5. Im, Jungho & Jensen, John. (2005). A change detection model based on neighborhood correlation image analysis and decision tree classification. Remote Sensing of Environment. 99. 326-340. 10.1016/j.rse.2005.09.008.
6. P. Lu, Y. Qin, Z. Li, A. C. Mondini, and N. Casagli, "Landslide mapping from multi-sensor data through improved change detection-based Markov random field,"
7. M. E. Zelinski, J. Henderson, and M. Smith, "Use of Landsat 5 for change detection at 1998 Indian and Pakistani nuclear test sites" *IEEE Trans. Geosci. Remote Sens.*
8. Seo, Y. H. Kim, Y. D. Eo, M. H. Lee, and W. Y. Park, "Fusion of SAR and multispectral images using random forest regression for change detection".
9. X. W. Chen, "Using remote sensing and GIS to analyse land cover change and its impacts on regional sustainable development," *Int. J. Remote Sens.*, vol. 23, no. 1, pp. 107–124, Jan. 2002.
10. Zhou, G. Cao, Y. Li, and Y. Shang, "Change detection based on conditional random field with region connection constraints in high-resolution remote sensing images," *IEEE J. Sel. Topics Appl. Earth Observ. Remote Sens.*
11. Saux, Bertrand & Randrianarivo, Hicham. (2013). Urban change detection in SAR images by interactive learning. International Geoscience and Remote Sensing Symposium (IGARSS). 3990-3993. 10.1109/IGARSS.2013.6723707.
12. Ouerghi, "A deep learning model for change detection on satellite images," *Image Processing Online*, vol. 12, pp. 550–557, 2022.
13. T. Chen, Z. Lu, Y. Yang, and Y. Zhang, "A Siamese network-based U-Net for change detection in high-resolution remote sensing images".
14. H. Lyu and H. Lu, "Learning a transferable change detection method by recurrent neural network," in *Proc. IEEE Int. Geosci. Remote Sens. Symp.*, 2016, pp. 5157–5160.
15. B. C. Pijanowski, D. G. Brown, B. A. Shellito, and G. A. Manik, "Using neural networks and GIS to forecast land use changes: A land transformation model".
16. X. X. Zheng and T. Chen, "High spatial resolution remote sensing image segmentation based on the multiclassification model and the binary classification model," *Neural Comput. Appl.*, pp. 1–8, 2021, doi:[DOI].
17. H. Cai, T. Chen, R. Q. Niu, and A. Plaza, "Landslide detection using densely connected convolutional networks and environmental conditions," *IEEE J. Sel. Topics Appl. Earth Observ. Remote Sens.*

18. X. Wang, K. Tan, Q. Du, Y. Chen, and P. Du, "CVA2E: A conditional variational autoencoder with an adversarial training process for hyperspectral imagery classification".

19. R. C. Daudt, B. Le Saux, A. Boulch, and Y. Gousseau, "Urban change detection for multispectral Earth observation using convolutional neural networks".

20. S. Zagoruyko and N. Komodakis, "Learning to compare image patches via convolutional neural networks," in *Proc. IEEE Conf. Comput. Vis. Pattern Recognit.*, 2015, pp. 4353–4361.